

Measuring the spatiotemporal electric field of ultrashort pulses with high spatial and spectral resolution

Pamela Bowlan,^{1,*} Pablo Gabolde,¹ Matthew A. Coughlan,² Rick Trebino,¹ and Robert J. Levis²

¹*School of Physics, Georgia Institute of Technology, 837 State Street NW, Atlanta, Georgia 30332, USA*

²*Department of Chemistry, Center for Advanced Photonics Research, Temple University, Philadelphia, Pennsylvania 19122, USA*

*Corresponding author: PamBowlan@gatech.edu

Received November 2, 2007; revised January 20, 2008; accepted January 22, 2008;
posted March 4, 2008 (Doc. ID 89285); published May 7, 2008

We demonstrate an experimentally simple and high-spectral-resolution version of spectral interferometry (SEA TADPOLE) that can measure complicated pulses (in time) at video rates. Additionally, SEA TADPOLE can measure spatial information about a pulse, and it is the first technique that can directly measure the spatiotemporal electric field $[E(x, y, z, \lambda)]$ of a focusing ultrashort pulse. To illustrate and test SEA TADPOLE, we measured $E(\lambda)$ of a shaped pulse that had a time–bandwidth product of approximately 100. To demonstrate that SEA TADPOLE can measure focusing pulses, we measured $E(x, \lambda)$ at and around the focus produced by a plano–convex lens. We also measured the focus of a beam that had angular dispersion present before the lens. We have found that SEA TADPOLE can achieve better spectral resolution than an equivalent spectrometer, and here we discuss this in detail, giving both experimental and simulated examples. We also discuss the angular acceptance and spatial resolution of SEA TADPOLE when measuring the spatiotemporal field of a focusing pulse. © 2008 Optical Society of America
OCIS codes: 320.7100, 260.3160, 320.4550.

1. INTRODUCTION

A. Measuring Pulses with Complex Spectral Fields

Many applications of ultrashort pulses, from coherent control [1,2] to multiphoton microscopy [3,4], utilize very complicated shaped pulses. To optimize these experiments, it is important to be able to completely characterize these complicated pulses. Also, such experiments often require the use of feedback loops to select the appropriate pulse shape, and usually pulse measurement is a necessary part of these loops. Therefore a fast (video-rate) pulse-measurement technique for measuring shaped pulses would benefit coherent control experiments.

Only three techniques have proven capable of measuring complex pulses: frequency-resolved optical gating (FROG) [5], cross-correlation FROG (XFROG) [6], and (linear) spectral interferometry (SI). We consider FROG methods for measuring complex pulses in a separate paper in this issue [7], but it is worth noting here that FROG techniques, while quite fast for simple pulses (time–bandwidth product $< \sim 10$), can be slow (> 1 s for convergence) when the pulse is complex. SI has the advantage that it is inherently a single-shot technique and the interferogram can be directly and quickly inverted regardless of the complexity of the pulse. Therefore SI could in principle be used to measure very complicated pulses in real time. Another useful property of SI is that it is a linear technique, and so it is extremely sensitive and can measure pulses that are approximately 9 orders of magnitude weaker than those that can be measured using nonlinear-optical methods [8]. SI's only fundamental

drawback is that it requires a previously measured reference pulse whose spectrum contains that of the unknown pulse. Fortunately, when measuring shaped pulses, the unshaped pulse provides an ideal such reference pulse, and it is easily measured using another technique, such as FROG or its experimentally simpler version, GRENOUILLE.

Unfortunately, traditional SI has a few practical limitations that have prevented it from working well for this application. The standard reconstruction algorithm for SI, often referred to as Fourier transform spectral interferometry (FTSI), involves introducing a delay between the interfering pulses and then Fourier filtering the data along the time axis. Reconstructing the field in this way results in a loss of spectral resolution that is typically a factor of 5. Thus, very bulky (~ 1 m) high-resolution spectrometers are required for measuring the longer shaped pulses (which can be as long as 10 ps). Another important practical problem with SI is that it has extremely strict alignment requirements, such as perfectly collinear beams with similar intensities and identical spatial modes, so its alignment must be frequently tweaked. SI would be very useful for measuring shaped pulses if these two problems could be overcome.

Fortunately, it is possible to overcome the loss of resolution experienced with FTSI by crossing the pulses at an angle to yield interference fringes versus position, x_c [9–14], and measuring a 2D interferogram versus camera position (x_c) and wavelength (λ). In this device, the pulses are temporally overlapped, so only enough spectral reso-

lution to measure the pulse is required (unlike FTSI, which requires higher resolution to resolve the spectral interferogram). In this case, the measured interferogram $I(x_c, \lambda)$ is given by

$$S(\lambda, x_c) = S_{\text{ref}}(\lambda) + S_{\text{unk}}(\lambda) + 2\sqrt{S_{\text{ref}}(\lambda)}\sqrt{S_{\text{unk}}(\lambda)} \times \cos[2kx_c \sin \theta + \varphi_{\text{unk}}(\lambda) - \varphi_{\text{ref}}(\lambda)]. \quad (1)$$

In the above equation, θ is the half-crossing angle. The spectral intensity and phase of the unknown pulse can then be retrieved from Eq. (1) by Fourier filtering the interferogram along the x_c axis, and, as a result, the unknown pulse is reconstructed with the full resolution of the spectrometer [9].

We recently introduced an interferometer based on this idea, which we call SEA TADPOLE or spatially encoded arrangement for temporal analysis by dispersing a pair of light e-fields [15]. In SEA TADPOLE, in addition to reconstructing the unknown field with the full resolution of the spectrometer, we also use a simple experimental setup (using optical fibers) that makes the device insensitive to misalignments and easy to use. Using SEA TADPOLE, we have shown that pulses with time–bandwidth products (TBPs) as large 400 could be measured, and others have since shown that SEA TADPOLE is useful for measuring shaped pulses [16]. Additionally, we even found that, for many pulses, the spectrum that we retrieve from the interferogram is better resolved than the spectrum that we measure directly with the spectrometer in SEA TADPOLE, and this improvement can be as great as a factor of 7 (in the sense that the spectral fringe contrast was 7 times better in the SEA TADPOLE spectrum) [15].

B. Measuring the Spatiotemporal Field of Focusing Pulses

Nearly all ultrashort pulses are utilized at a focus, where their intensity is high. And in addition to their possible complexity in time and frequency, focused pulses can easily have complex spatiotemporal structure, especially if lens aberrations are present [17–20]. Simulations have shown that it is difficult, if not impossible, to avoid group delay dispersion and pulse lengthening due to lens aberrations, which result in radially varying group delay, for example. When these distortions are present, adequate material-dispersion compensation is difficult, and the pulse will not have a transform-limited pulse duration even with perfect material-dispersion compensation. This is especially important in fields such as nonlinear microscopy and micromachining. Because the focus can easily contain spatiotemporal distortions (and severe ones at that), simply making a measurement of the time- or frequency-dependent spectral intensity and phase is not a sufficient characterization of the pulse; a complete spatiotemporal measurement must be made at the focus. And because the pulse can be complex in both space and frequency (time), the measurement technique must have both high spatial and high spectral resolution.

Measuring the spatiotemporal field of a pulse at a focus is a difficult problem, and previous pulse measurement techniques are only able to measure the focused pulse versus time averaged over space or vice versa [21–23]. With two-dimensional spectral interferometry it is possible to

measure the spatiotemporal field of the recollimated focused pulse (by double passing the focusing lens), and this information can be used to numerically backpropagate the focused pulse to determine the spatiotemporal field at the focus by dividing the measured phase by 2. Drawbacks to this approach are that the pulse must be perfectly recollimated, it is difficult to measure aberrations due to misalignment of the lens, and the method is quite indirect: One has to assume that the numerical backpropagation is correct [24].

Recently we demonstrated that SEA TADPOLE can be used to measure the spatiotemporal field of focusing ultrashort pulses [25]. Because the entrance to SEA TADPOLE is a single-mode fiber, it naturally measures pulses with high spatial resolution, and the measurement can be made at the focus. If we use a fiber with a mode size smaller than the focused spot size, then we can make multiple measurements of $E_{\text{unk}}(\lambda)$ by scanning the fiber longitudinally and transversely, so that we measure $E_{\text{unk}}(x, y, z, \lambda)$ at and around the focus.

2. EXPERIMENTAL DETAILS AND RETRIEVAL

A. SEA TADPOLE Experimental Setup

To measure $E_{\text{unk}}(\lambda)$ using SEA TADPOLE, we couple the reference and unknown pulses into two identical fibers. The output ends of the fibers are placed close together, so that when the light diverges from them, both beams are collimated with the same spherical lens (focal length f). Because the fibers are displaced from the optic axis (with a distance d between them, which is usually <1 mm), the collimated beams cross at angle θ , which is equal to d/f , and we place a camera at the crossing point in order to record their interference. In the other dimension we use a diffraction grating and a cylindrical lens to map the wavelength onto the horizontal position (as in a conventional spectrometer) so that we record a 2D interferogram given by Eq. (1). Figure 1 illustrates the experimental setup. Note that, when we are using SEA TADPOLE to measure $E_{\text{unk}}(\lambda)$ of a pulse that is free of spatiotemporal couplings, the scanning stage shown in Fig. 1 is not necessary (so this fiber is left stationary, and only one interferogram is needed). Typical experimental parameters include a crossing angle of 0.06 deg; a camera with approximately 10^6 pixels, each $4.7 \mu\text{m}^2$ in area; a collimating lens with a focal length of 150 mm; and 40 cm long fibers with a mode size of $5.6 \mu\text{m}$, and we typically build the spectrometer to have a range of 80 nm and a spectral resolution of approximately 0.14 nm (as we will show later). The range of the wavelength axis can be decreased in order to increase the spectral resolution simply by using a longer focal length cylindrical lens, as in any spectrometer, and the usual limitations of grating spectrometers apply.

The only requirements on the reference pulse in SEA TADPOLE are that it be from the same laser so that the interfering pulses are coherent (time synchronized), and its spectrum must contain that of the unknown pulse (otherwise the spectral-interference term is zero at that frequency). The best reference pulse is generally the pulse taken directly out of the laser, because this is usually a spatially and spectrally smooth pulse that is easy to mea-

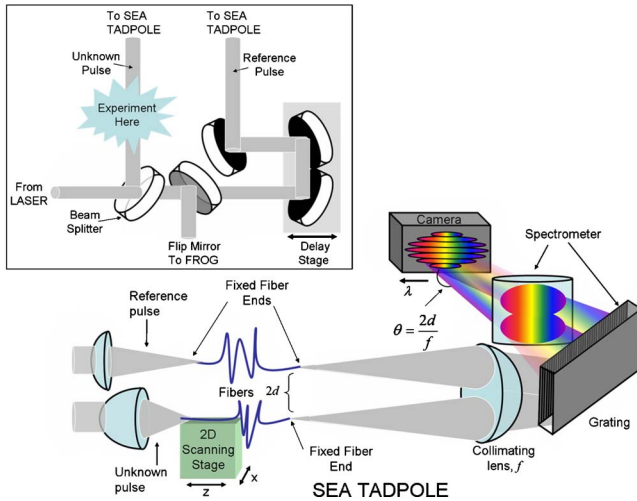


Fig. 1. (Color online) SEA TADPOLE experimental setup. A reference pulse and an unknown pulse are coupled into two single-mode fibers with approximately equal lengths. At the other end of the fibers, the diverging beams are collimated using a spherical lens (f). After propagating a distance f , the collimated beams cross and interfere, and a camera is placed at this point to record the interference. In the other dimension, a grating and a cylindrical lens map wavelength onto the camera's horizontal axis (x_c).

sure using FROG or GRENOUILLE [26]. The image at the top of Fig. 1 illustrates this. If it is only necessary to determine the phase and spectrum introduced by an experiment such as some material, a lens, or a pulse shaper, then it is not necessary to characterize the reference pulse.

When using SEA TADPOLE to measure the spatiotemporal field, $E_{\text{unk}}(x, y, z, \omega)$, the scanning stage shown in Fig. 1 is used to move the entrance to the unknown pulse's fiber transversely and longitudinally so that multiple interferograms are measured all along the cross section and length of the incoming beam. This allows us to

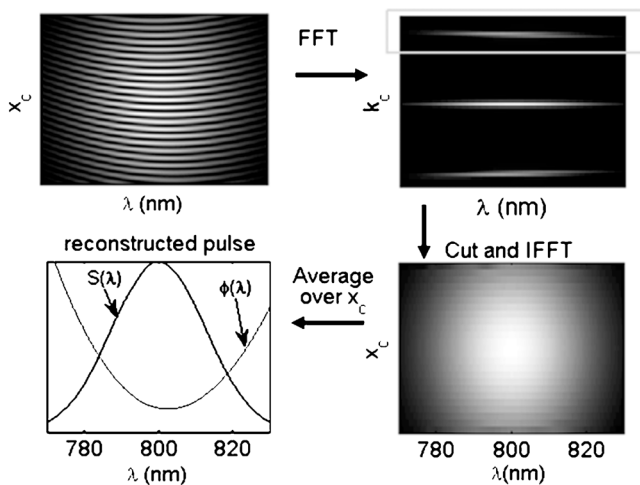


Fig. 2. SEA TADPOLE retrieval. The top left image is a typical interferogram, which is Fourier transformed from the λ - x_c to the λ - k_c domain where only one of the sidebands is then used. This sideband is then inverse Fourier transformed back to the λ - x domain. The result is then averaged over x_c , and the reference pulse is divided out in order to isolate the intensity and phase of the unknown pulse.

reconstruct $E_{\text{unk}}(\lambda)$ versus x, y , and z in the focal region, so that the spatiotemporal field of the focusing beam, $E_{\text{unk}}(x, y, z, \lambda)$, can be reconstructed. Scanning the entrance fiber to SEA TADPOLE can be used to measure the spatiotemporal field of focusing or collimated beams as long as the collimated beam is intense enough to be detected after being sampled by the fiber. As we will discuss in Section 6, the spatial resolution of scanning SEA TADPOLE, or the tightest focus that SEA TADPOLE can measure with a given fiber, is given by the NA of the fiber, and, the fiber that we used had a NA of 0.12. For more details about scanning SEA TADPOLE, please see [15].

B. Retrieving the Spectrum and Phase from the SEA TADPOLE Trace

The unknown electric field is reconstructed from the interferogram much like that described in [9,15]. First we take a 1D Fourier transform of the 2D interferogram with respect to the camera's position axis, so that the Eq. (1) becomes

$$S_{\text{ref}}(\lambda) + S_{\text{unk}}(\lambda) + E_{\text{unk}}(\lambda)E_{\text{ref}}^*(\lambda)\delta\left(k_c + 2\frac{2\pi}{\lambda}\sin\theta\right) + E_{\text{unk}}^*(\lambda)E_{\text{ref}}(\lambda)\delta\left(k_c - 2\frac{2\pi}{\lambda}\sin\theta\right). \quad (2)$$

As a result, the data separate into three bands (in k_c) in which each of the two sidebands contains the complex field of the unknown pulse, and we can extract the required information from either of these. The sidebands are slightly tilted because the argument of the delta function is wavelength dependent, and hence the fringe spacing in the x_c domain is wavelength dependent. Although we could isolate the unknown spectral field at this point, it is easier to inverse Fourier transform back to the x_c domain where the tilt becomes a small, linear phase term given by $[(2x\sin\theta)/c](\omega - \omega_0)$, which is usually small enough to neglect. At this point $E_{\text{unk}}(\lambda)$ can be obtained in several ways (summing, taking one line, or averaging), and we have found that what works best (especially in the presence of noise) is to average the 2D data over x_c and then divide out the reference electric field. Figure 2 illustrates the retrieval of $E_{\text{unk}}(\lambda)$.

C. Other Issues and Comments

As long as the experimental setup is considered, there is no direction of time ambiguity in SEA TADPOLE. If the unknown pulse enters the device from the bottom fiber, then the phase difference will have the sign shown in Eq. (1), and it will have the opposite sign if the unknown pulse enters through the top fiber. It is also necessary to consider which interference term (in our analysis we used the top one) is used in the reconstruction because these are complex conjugates of one another so their spectral phase differences have opposite signs as illustrated by Eq. (2).

In previous publications, we have already mentioned that a calibration can be performed if the spectral phase difference between the two arms of the interferometer is not zero (possibly due to different fiber lengths) [15,25]. This is simply done by measuring the spectral-phase dif-

ference between the two arms of the interferometer when the unknown arm also contains the reference pulse, and then this phase can be subtracted out from all subsequent measurements. In principle, the phase difference in the interferometer as a function of x_c and ω can be measured so that any spatial phase difference introduced by the interferometer is also removed. In practice, because an interferometer only measures phase differences and both beams travel through the same optics and similar fibers, we find that it is not necessary to do the 2D calibration.

3. USING SEA TADPOLE TO MEASURE SHAPED PULSES

Previous work has shown that SEA TADPOLE (without fibers) is useful for measuring shaped pulses [16]. To further demonstrate this, we used SEA TADPOLE to measure a phase-shaped pulse, which was shaped using a 256-element LCD pulse shaper. For this experiment, we used an 85 MHz repetition rate KM Labs Ti:sapphire oscillator, which had approximately 30 nm of bandwidth. For the reference pulse, we used the unshaped oscillator pulse so that the phase difference that we measured with SEA TADPOLE was the phase introduced by the pulse shaper. Figure 3 shows the results of this experiment. Figure 3(b) shows the phase that was applied by the shaper and the phase that was measured by SEA TADPOLE, and you can see that the two are in good agreement. Figure 3(c) shows the reconstructed spectrum

$[S_{\text{unk}}(\lambda)]$ compared with the spectrometer measurement $[S_{\text{sp}}(\lambda)]$, where $S_{\text{sp}}(\lambda)$ was measured using the spectrometer in SEA TADPOLE by blocking the reference pulse. You can see that $S_{\text{unk}}(\lambda)$ is essentially a better-resolved version of $S_{\text{sp}}(\lambda)$ as is often the case in SEA TADPOLE (we discuss this in detail in Section 5). Figure 3(d) shows the reconstructed temporal field, and you can see that this pulse had a TBP of approximately 100. Figure 3(a) is the SEA TADPOLE trace, and it nicely illustrates that the curvature of the fringes is the phase difference between the interfering pulses.

4. MEASURING FOCUSING PULSES

In a previous paper we showed that SEA TADPOLE could accurately measure the spatiotemporal field of focusing pulses [25]. Here we have done additional experiments to further demonstrate this capability. We measured $E_{\text{unk}}(x, \lambda)$ at nine different longitudinal positions (z) in the focal region produced by a BK7 lens with a focal length of 25 mm. The NA of the focus was 0.085 (using the $1/e^2$ full width of the beam before the lens). The input pulse had a bandwidth of 30 nm (FWHM), and we used a KM Labs Ti:sapphire laser with a center wavelength of 800 nm. To verify that this measurement was correct, we propagated a Gaussian pulse through a lens using the experimental parameters listed above. For the numerical propagation, we used the Fresnel approximation to Huy-

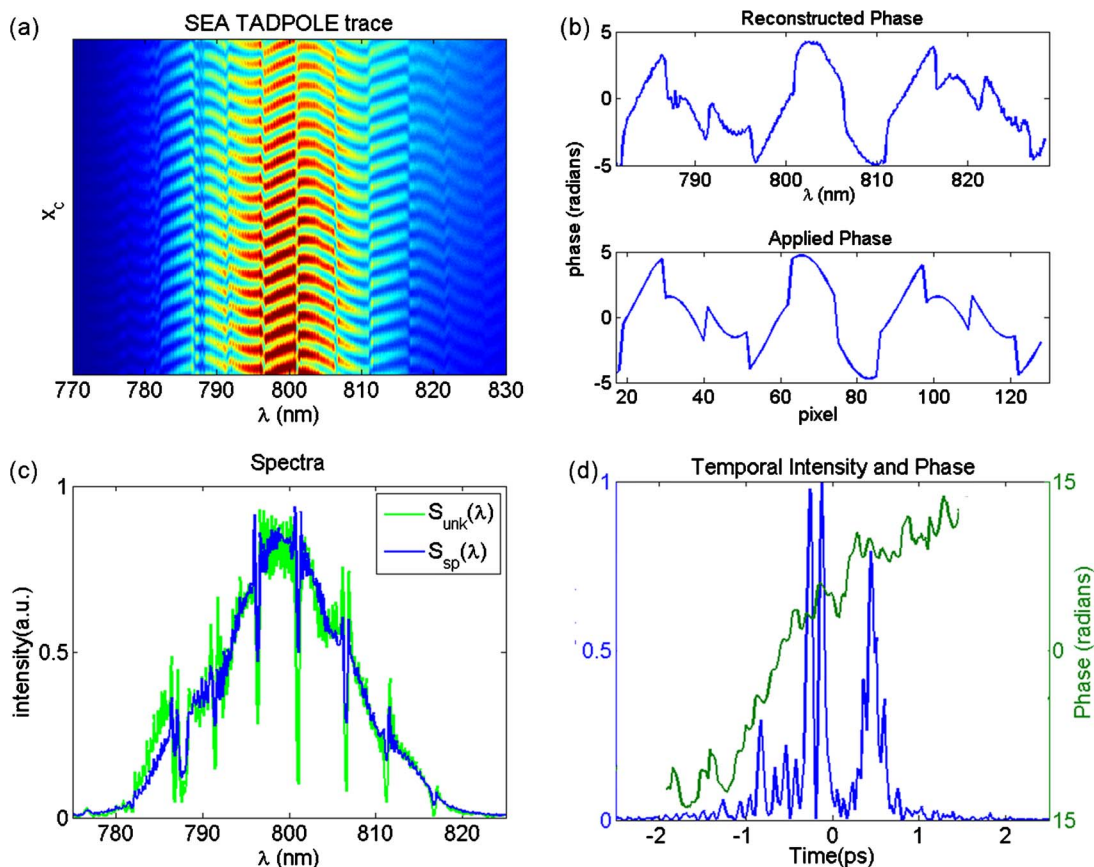


Fig. 3. (Color online) (a) SEA TADPOLE trace for a shaped pulse. (b) Retrieved spectral phase compared with the phase applied to the shaper. (c) Retrieved spectrum (S_{unk}) compared with the spectrometer spectrum (S_{sp}). (d) Retrieved temporal intensity and phase.

gens integral [27], which is valid for this numerical aperture. Figure 4 displays the results of this experiment.

The simulations and experiments shown in Fig. 4 are in good agreement. The ripples before the focus are due to the spherical aberrations introduced by the lens. This lens also has chromatic aberrations present, which cause the pulse fronts to be asymmetric about the focus. The color in the plots displays the instantaneous frequency (see the color bar in Fig. 4), and it shows that the redder colors are ahead of the bluer colors, which is due to the material dispersion of the lens. Although there should be some color variation due to chromatic aberrations, this is not noticeable because it is much smaller than that due to group delay dispersion (for an example where this is noticeable see [25]). The aberrations in this lens increase the focused spot size by a factor of 3.

To further demonstrate scanning SEA TADPOLE, we focused a beam that had angular dispersion and then measured the spatiotemporal field in and around the focus. To introduce angular dispersion, we used the -1 order of a ruled reflection grating (300 grooves/mm), which we placed just before (by 17.5 cm) the focusing lens. We also simulated this experiment by calculating $E_{\text{unk}}(x, \lambda)$ just before the lens using Kostenbauder matrices [28,29], and then we numerically propagated this beam through the lens and to the focal region just as described above. The results of this experiment are shown in Fig. 5. Again, the experiment and simulation are in good agreement. Because a lens is a Fourier transformer, the angular dispersion introduced by the grating becomes spatial chirp at the focus. As a result, the pulse front becomes flat at the focus, because the pulse front tilt in this case is due to angular dispersion. Because the magnification of the optical system becomes negative after the focus, the order of the colors and the sign of the pulse front tilt change after the focus. This measurement essentially shows the pulse in the focal region of a spectrometer. The lens that we used in this experiment is the aspheric lens described in [25].

In these measurements, we found the measured difference in the interferometer due to the lens at each fiber position. We did not remove the phase of the reference pulse in these measurements because we were interested only in the phase of the focused pulse (the phase introduced by the lens). This is appropriate for characterizing lenses because it shows the distortions introduced by the lens for a given NA and bandwidth.

The data shown in Figs. 4 and 5 took approximately 30 min to collect.

5. SPECTRAL RESOLUTION OF SEA TADPOLE

A. Introduction

In a previous publication [15], and in Fig. 3, we showed that the spectrum retrieved from the SEA TADPOLE interferogram [$S_{\text{unk}}(\lambda)$] can be better resolved than the spectrum measured directly with the same spectrometer that is used in the SEA TADPOLE device. Experimentally we make this comparison by measuring the spectrometer spectrum [$S_{\text{sp}}(\lambda)$] simply by blocking the SEA TADPOLE reference beam, and $S_{\text{unk}}(\lambda)$ comes from the interference

term as described in Section 2. Our measured SEA TADPOLE $S_{\text{unk}}(\lambda)$ spectra have exhibited a factor of 7 better spectral resolution than the corresponding spectrometer spectra—a significant improvement in spectral resolution [15]. Of course, interferometry can be used to improve spatial resolution as well as spectral resolution [30]. In spectral interferometry (FTSI) this spectral resolution improvement does not occur (or it is not noticeable). Indeed, due to the required pulse separation and Fourier filtering on the time axis, FTSI actually experiences a spectral-resolution loss of a factor of ~ 5 [8,31,32].

In the following subsections, we will discuss in detail the spectral resolution of SEA TADPOLE, which is significantly better than that of a spectrometer for some pulses (such as a double pulse). Also, there are some cases where the spectrometer spectrum is more accurate than the SEA TADPOLE spectrum.

B. Simulations

The resolution improvement achieved by interferometry can be explained by looking at one of the interference terms, given by $E_{\text{unk}}(\lambda)E_{\text{ref}}^*(\lambda)$. We consider only the case of a reference pulse with a simple or smooth spectrum used to measure a much more complicated unknown pulse, and for this discussion we will assume that the reference pulse has a flat spectral phase (although this is not required) and that it is at zero delay, which is usually the case in experiments. Then the interference term is approximately equal to $E_{\text{unk}}(\lambda)$, or the complex electric field of the unknown pulse. As a result, SEA TADPOLE directly measures the unknown electric field, while a spectrometer measures $|E_{\text{unk}}(\lambda)|^2$, or its magnitude squared.

To see why these two measurements can result in different spectra, we must include the effect of the spectrometer's instrument response function, $H(\lambda)$, whose width is the spectral resolution of the spectrometer ($\delta\lambda$). The finite resolution of the spectrometer effectively smears out or averages together neighboring frequency components in the measured quantity, which can be modeled as a convolution [33,34]. Therefore, the spectrometer spectrum is given by $|E_{\text{unk}}(\lambda)|^2 \otimes H(\lambda)$, and the SEA TADPOLE spectrum is given by $|E_{\text{unk}}(\lambda) \otimes H(\lambda)|^2$.

From the above expressions, it is immediately apparent that, if the amplitude of E_{unk} is very narrow compared with H , and H is a Gaussian, then the measured spectral width (or the width of the function that the measured signal is convolved with) will be $\sqrt{2}$ narrower in SEA TADPOLE than with a standard spectrometer (see Fig. 7). Also consider that the eigenfunction of the convolution operator is $\exp(i\omega\tau)$, so any measurement using SEA TADPOLE where $E_{\text{unk}}(\omega)$ is a purely oscillatory function (such as a double pulse, which is approximately a purely oscillatory function when the spacing between two pulses is longer than the pulse duration of the individual pulses) would yield a perfect measurement of the field and hence also the spectrum, independent of H , remarkably. Because a standard spectrometer measurement of such a spectrum would still be broadened in the usual manner, SEA TADPOLE yields significantly better spectral resolution in this case. In general we expect the improvement in spectral resolution offered by SEA TADPOLE to vary

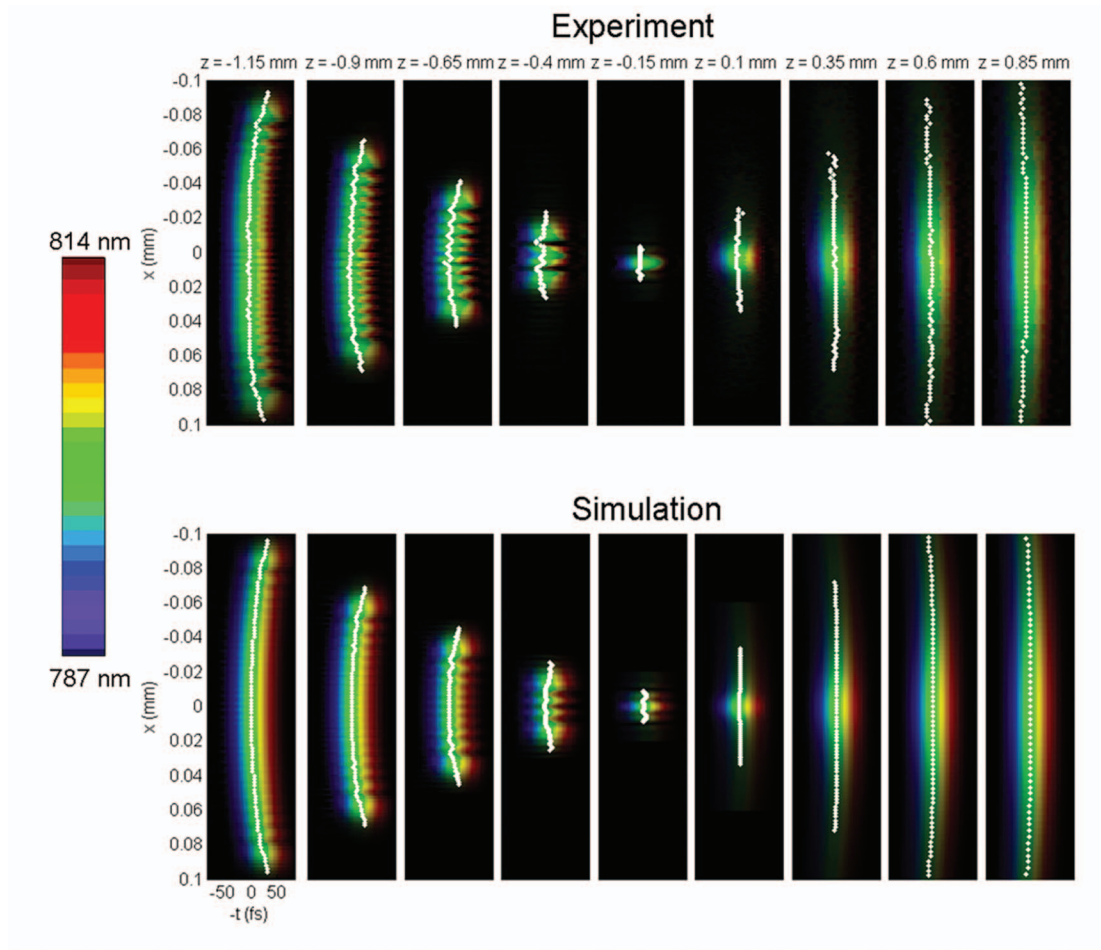


Fig. 4. $E(x, z, t)$ in the focal region of a plano-convex lens. The experimental results are displayed in the top plots, and the simulations are shown in the bottom plots. Each box displays the amplitude of the electric field versus x and $-t$ at a distance z from the geometric focus. The white dots show the pulse fronts, or the maximum temporal intensity for each value of x . The color represents the instantaneous frequency, which shows that the redder colors are ahead of the bluer colors due to material dispersion.

with the shape of the pulse involved and be somewhere in the middle of that described for the two cases above.

If we view the effect of finite spectral resolution in the time domain, the measured signal versus time is multiplied by the temporal response function $h(t)$ [the Fourier transform of $H(\lambda)$], and we can interpret this as a finite time window. Therefore, when using SEA TADPOLE, the pulse duration of E_{unk} has to be less than the width of the time window, ΔT . When using a spectrometer, the width of the pulse's temporal field autocorrelation [$E_{\text{unk}}(t) \otimes E_{\text{unk}}(t)$] has to be less than ΔT , and most of the time this will be a wider function than $E_{\text{unk}}(t)$ itself. If we assume that the spectral response function is Gaussian, then the width of the time window is related to the spectral resolution by $\Delta T = 2\lambda^2/c\delta\lambda$, which is useful for determining the spectral resolution needed to measure a given pulse.

An important difference between SEA TADPOLE and a spectrometer measurement is that the spectral phase of $E_{\text{unk}}(\lambda)$ can have no effect on $S_{\text{sp}}(\lambda)$ (because standard spectrometers cannot measure phase information), but for $S_{\text{unk}}(\lambda)$ this is not true. Because SEA TADPOLE resolves the complex field, the spectral resolution of the spectrometer should, in general, be smaller than the

smallest feature in the pulse's spectral amplitude and its spectral phase (or equivalently, just its complex field) in order to make an accurate measurement. Another way to say this is that, because the convolution acts on the unknown pulse's complex field, it can mix together the spectrum and phase (which can distort the retrieved spectrum or phase). When the spectral phase has features that are too small to be resolved by the spectrometer, then its spectrum cannot be accurately measured using the interferometer (nor can its phase), but a spectrometer could still measure this pulse's spectrum. Therefore, as long as the pulse's complexity comes from its spectrum rather than its phase, $S_{\text{unk}}(\lambda)$ will essentially always be better resolved than $S_{\text{sp}}(\lambda)$.

Because the difference in $S_{\text{unk}}(\lambda)$ and $S_{\text{sp}}(\lambda)$ is pulse dependent, this is best illustrated using examples. Figure 6 shows a simulation of how $S_{\text{unk}}(\lambda)$ compares with $S_{\text{sp}}(\lambda)$ and the ideal spectrum for six different pulse shapes. In Fig. 6, the white curve shows the actual spectrum, $S_{\text{unk}}(\lambda)$ is shown in gray, and $S_{\text{sp}}(\lambda)$ is shown in black. In this simulation, we used a Gaussian spectral response function with a width of 0.3 nm, and all of the spectra are normalized to have an area of 1.

In Fig. 6(b), which was generated using a double pulse

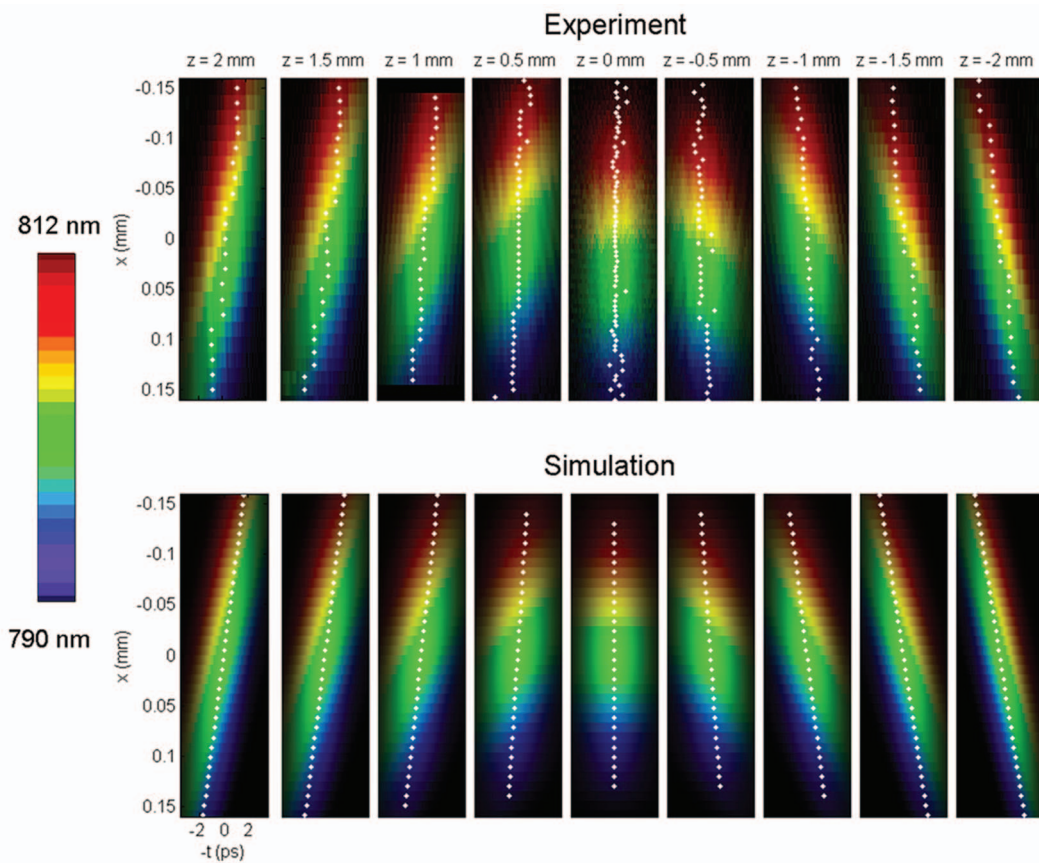


Fig. 5. $E(x, z, t)$ in the focal region of the beam that had angular dispersion. The data is displayed in the same way as in Fig. 4. The angular dispersion becomes purely spatial chirp at the focus because a lens is a Fourier transformer.

(such as that generated by a Michelson interferometer), $S_{\text{unk}}(\lambda)$ is identical to the real spectrum even though the duration of the double pulse is 50% of the width of $h(t)$. This is because double pulses that are approximately equal to two delta functions in time where one pulse is at $t = \tau$ and the other pulse is at $t = -\tau$ are unchanged by the temporal response function (except by a constant). Or as stated previously, double pulses are eigenfunctions of the convolution operator. As a result, very long double pulses can be perfectly resolved using SEA TADPOLE. Of course, the price to be paid is that, when the double pulse is long compared with $h(t)$, the eigenvalue is small, so the measured field is weak, and the signal can get lost in the noise [15].

Figures 6(a), 6(c), and 6(d) show more typical improvement that we see with SEA TADPOLE, and although $S_{\text{unk}}(\lambda)$ is not identical to the real spectrum, it is noticeably closer to this than $S_{\text{sp}}(\lambda)$ is.

Figures 6(e) and 6(f) show two examples in which $S_{\text{sp}}(\lambda)$ is identical to the real spectrum and $S_{\text{unk}}(\lambda)$ is distorted. These are pulses with Gaussian spectra and a sinusoidal spectral phase [Fig. 6(e)] and a huge amount of chirp [Fig. 6(f)]. So these pulses have simple spectra (that are easy to resolve with a spectrometer), but complex spectral phases that make their pulse durations very long in time [80% of $h(t)$ for Fig. 6(e) and 140% for Fig. 6(f)]. Therefore $S_{\text{unk}}(\lambda)$ is distorted, while a spectrometer can perfectly measure these spectra. Although we are accustomed to seeing smeared features in the spectrum when a spectrometer

lacks sufficient resolution to make the measurement, when SEA TADPOLE lacks resolution to resolve a pulse because it is too long compared with $h(t)$ due to its spectral phase, the distortions look quite different.

The numerical factor for the resolution difference in $S_{\text{sp}}(\lambda)$ and $S_{\text{unk}}(\lambda)$ depends on the exact shape of the pulse. For a Gaussian spectrum, squaring decreases the rms width by $\sqrt{2}$, which is the resolution improvement for SEA TADPOLE in this case (as long as the spectral phase is relatively small). Figure 7 shows the result of a simulation that illustrates the difference in the $S_{\text{sp}}(\lambda)$ and $S_{\text{unk}}(\lambda)$ for a spectrum that is a very thin Gaussian centered at 800 nm with a rms bandwidth of 0.1 nm. In Fig. 7 you can see that, although $S_{\text{unk}}(\lambda)$ is affected by the convolution, it is closer to the actual spectrum than $S_{\text{sp}}(\lambda)$. In this example, the rms width of $S_{\text{unk}}(\lambda)$ is 0.12 nm and, for $S_{\text{sp}}(\lambda)$, it is 0.16 nm, which is a difference of approximately $\sqrt{2}$ as expected.

C. Measurements

Additionally we can do some experimental tests of the resolution of SEA TADPOLE. First we experimentally measured the temporal response function of the spectrometer that we were using. We did this by observing the fringe visibility of the spectrum produced by an etalon as we increased the spacing between the two reflectors (reflectivity=57%), which is similar to the approach used in [34–36]. Quantitatively the change in visibility is most

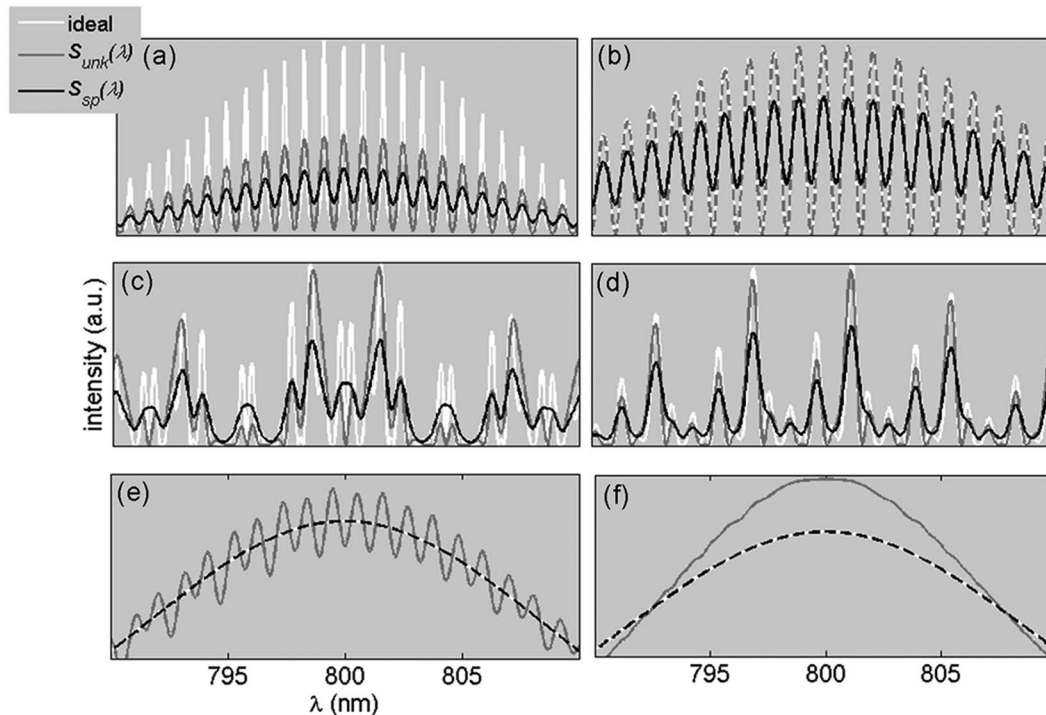


Fig. 6. Spectrum measured with a spectrometer (black) compared with that measured with SEA TADPOLE (gray) and the actual spectrum (white) (a) for a train of pulses, (b) for a double pulse, (c) for a sum of three double pulses with different delays, (d) for the same as (c) using shorter double pulses, (e) for a pulse with a Gaussian spectrum and a sinusoidal phase, and (f) for a very chirped Gaussian pulse. Please note that some of the curves are dashed to show that two curves are overlapping. In all cases, the color indicates the quantity.

easily determined by Fourier transforming the spectrum to the time domain and looking at the relative height of a sideband compared with the central peak. By measuring this relative height (which is attenuated due to the temporal response function) at different etalon spacings we can read off the temporal response function of the spec-

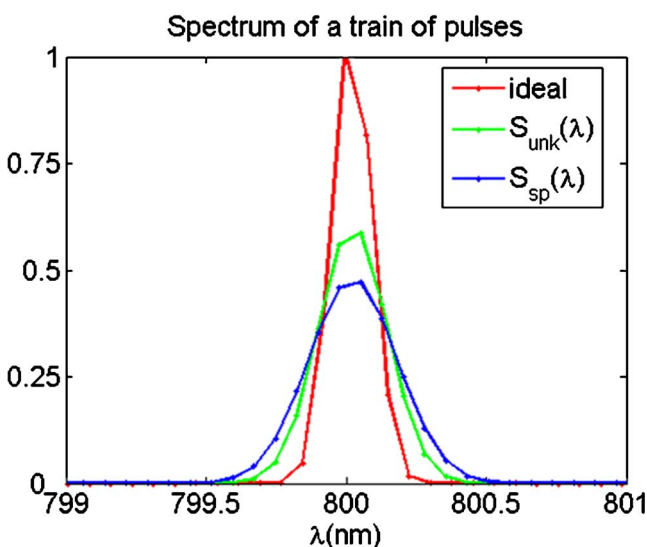


Fig. 7. (Color online) Spectrum retrieved from SEA TADPOLE (lightest or green) compared with the ideal spectrum (darker or red) and the spectrum measured with a spectrometer (darkest or blue). For this simulation both the spectral response function and the unknown pulse had a width of 0.1 nm.

trometer, and this result is shown in Fig. 8. The left side of Fig. 8 shows the measured temporal response function (dots) and a curve fit to the data (solid curve) and the rms width of $h(t)$ was 3.9 ps (FWHM of 6.2 ps). Because we know that $H(\lambda)$ is a real, symmetric function (we are using the spectrometer at the design wavelength), we know that $h(t)$ is symmetric, and therefore we only measured one side of the temporal response function. The right-hand plot in Fig. 8 shows the spectral response function, which was obtained by Fourier transforming $h(t)$, and this curve has a rms width of 0.14 nm and this spectrometer had a spectral range of approximately 80 nm. Therefore, if this spectrometer is used in SEA TADPOLE (assuming a relatively simple spectral phase) to measure $S_{\text{unk}}(\lambda)$, the smallest feature in $E_{\text{unk}}(\lambda)$ has to be greater than 0.14 nm, and if the spectrum $S_{\text{sp}}(\lambda)$ is measured directly with this spectrometer, the same restriction applies to $|E_{\text{unk}}(\lambda)|^2$, or the spectrum of the unknown pulse. Knowing the temporal response function is useful for determining precisely how well pulses can be measured using a given spectrometer in SEA TADPOLE. Additionally, the experimentally determined $H(\lambda)$ could be deconvolved from the reconstructed unknown field in order to further improve its resolution.

Figure 9 shows a typical experimental example of how $S_{\text{unk}}(\lambda)$ differs from $S_{\text{sp}}(\lambda)$ using the spectrometer that was characterized above and an unknown pulse comprising a train of pulses produced by an etalon. The left plot in Fig. 9 shows $S_{\text{sp}}(\lambda)$ and $S_{\text{unk}}(\lambda)$, and when comparing the two spectra we can see just as in Fig. 6(b), that $S_{\text{unk}}(\lambda)$ is a better-resolved version of $S_{\text{sp}}(\lambda)$. To verify that $S_{\text{unk}}(\lambda)$

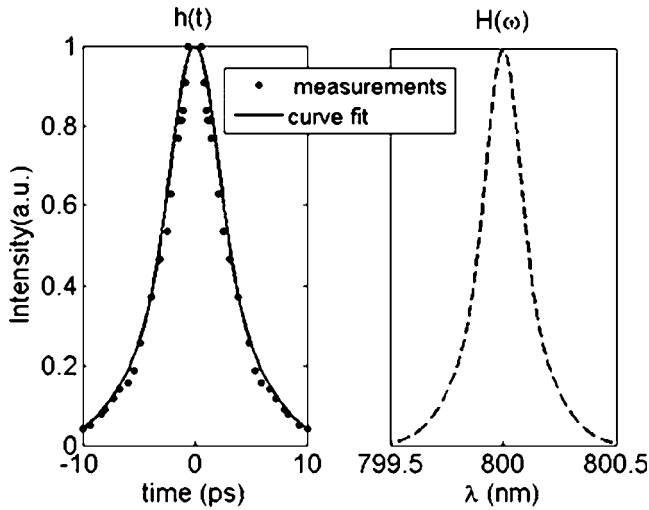


Fig. 8. The plot on the left shows the temporal response function that we measured (dots) using an etalon and the solid curve is a fit to this data. The plot on the right shows the Fourier transform of $h(t)$, which is the spectral response function. Note that we only measured this $h(t)$ on one side of the time axis because we expect it to be a symmetric function because $H(\omega)$ is a real function.

is more accurate than $S_{sp}(\lambda)$, we combined each of these spectra with the spectral phase that we retrieved from the SEA TADPOLE trace and Fourier transformed this to the time domain, and the right-hand side of Fig. 9 shows this result. Because we used an etalon with two identical 57% reflectors, the height of the second two peaks in the temporal intensity should be 0.33 and 0.11, respectively, so clearly the result from SEA TADPOLE is the more accurate one.

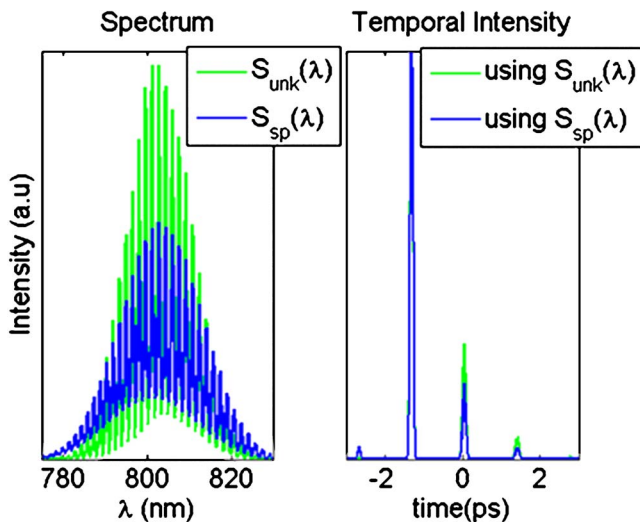


Fig. 9. (Color online) Experimental example of $S_{unk}(\lambda)$ versus $S_{sp}(\lambda)$. For this example we used an etalon with two identical reflectors both having a reflectivity of 57%. The plot on the right shows the two spectra where the darker (blue) one is $S_{sp}(\lambda)$ and the lighter (green) one is $S_{unk}(\lambda)$. The plot on the right shows the temporal intensity that was computed using $S_{sp}(\lambda)$ (darker or blue curve) and $S_{unk}(\lambda)$ (lighter or green curve). Because we know what these relative amplitudes should be, we can verify that the lighter (green) curve is more accurate than the darker (blue) curve.

Figure 3(c) (which was discussed in Section 3) shows another experimental example of how $S_{sp}(\lambda)$ compares with $S_{unk}(\lambda)$, which represents a significant improvement and illustrates the typical improvement that we expect for complicated pulses.

D. Other Issues and Comments

Another issue that must be considered when retrieving the spectrum from the SEA TADPOLE interferogram is the delay, or the location of $|E_{unk}(t)|$ underneath the temporal window. For example, if the unknown pulse is delayed with respect to the reference pulse (which is at zero delay) by τ , then the interference term becomes $E_{unk}(t - \tau) \otimes h(t)$ and is no longer centered underneath the temporal response function. Because the temporal window is flattest at its center, the unknown field will be more distorted by the temporal response function if it does not have a mean of zero because it will then be multiplied by a steeper part of $h(t)$. To illustrate this, we performed a simulation, making SEA TADPOLE traces for a double pulse at several different delays. The temporal intensity and spectra retrieved from these three traces are shown in Fig. 10. The bottom plot in Fig. 10 shows $h(t)$ (dashed curve), the ideal temporal intensity (dark curve), and the reconstructed temporal intensity (light curve), which is $|E_{unk}(t)|h(t)$. The higher plots show the reconstructed temporal intensity when the unknown pulse was delayed by 1 ps (middle) and 2 ps (upper), and these results are much more distorted than the result of the zero-delay interferogram. It is evident that it is important to measure the SEA TADPOLE interferogram at zero delay in order

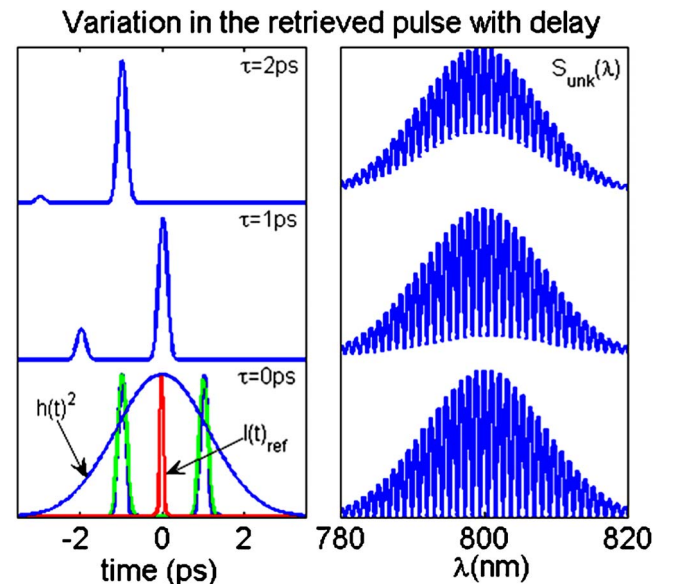


Fig. 10. (Color online) Variation in the reconstructed temporal intensity with delay (simulation): The bottom plot on the left shows the temporal response function, the reference pulse and the real (light or green curve) and the reconstructed temporal intensities (dark or blue curve). The top two left plots show how the reconstructed temporal intensity becomes distorted as the unknown pulse is delayed. The plots on the right are the spectrum retrieved from SEA TADPOLE at the three different delays. For this simulation we used an unknown pulse with a Gaussian spectrum (rms bandwidth of 8.5 nm) and a sinusoidal phase (with a frequency of 2500 fs⁻¹).

to minimize the damage done by the spectrometer's response function, and this becomes more important as the duration of the unknown pulse becomes close to the width of the temporal window.

6. SPATIAL RESOLUTION OF SEA TADPOLE

A. Introduction

When using scanning SEA TADPOLE to collect spatial information about a focusing pulse, a few questions arise. For example, what is the spatial resolution achieved by sampling the beam with a fiber, and what is the acceptance angle of the fiber? In a previous paper [25], we argued that these two questions are equivalent in SEA TADPOLE, and so if a SEA TADPOLE device has sufficient spatial resolution to sample a given focus, then it also has sufficient angular acceptance to measure that focus. In this section we consider this issue in more detail, further clarifying this point.

B. Spatial Resolution and Acceptance Angle of a Single-Mode Fiber

To determine the acceptance angle and spatial resolution of the fiber, we consider the effect of the fiber's finite spatial resolution as a convolution just as we did with the spectral resolution. For this discussion, we will ignore the effects of the finite spectral resolution. The measured spatiotemporal field in SEA TADPOLE is given by $E(x, \lambda)_{\text{unk}} \otimes H(x)$, and we will assume that the fiber's spatial resolution along the x and y axes is the same so that we can consider only one transverse spatial dimension. Now if we Fourier transform the resolved field to the k domain, we have $E(k, \lambda)_{\text{unk}} h(k)$, where $h(k)$ is the Fourier transform of $H(x)$. The function $h(k)$ can be viewed as an angular window, just as the temporal response function forms a time window. This product of the field with the angular response function is zero anywhere that $h(k)$ is zero, so only a certain range of k vectors will be coupled into the fiber. Therefore, because the fiber has a finite spatial resolution, it will also have a finite acceptance angle, and knowledge of the spatial resolution will yield the acceptance angle and vice versa.

To determine the acceptance angle of a single-mode fiber, we calculate the power transmitted into the fiber:

$$T = \left[\int dy \int dx E_{\text{fiber}}(x, y) E_{\text{unk}}^*(x, y) \right]^2. \quad (3)$$

This integral is a measure of the spatial overlap of the mode of the fiber with the mode of the unknown pulse [37,38]. $E_{\text{fiber}}(x, y)$ is approximately equal to a Gaussian with a width (full width at e^{-1}) equal to the single-mode field diameter d of the fiber. For a Gaussian beam with a waist size (diameter) w (where $w > d$) with an incident angle into the fiber (with respect to the fiber axis) of θ , it has been shown [38] that the power coupled into the fiber as a function of θ is given by

$$T(\theta) = \left(\frac{2dw}{d^2 + w^2} \right)^2 \exp \left[- \frac{2(\pi wd\theta)^2}{(w^2 + d^2)\lambda^2} \right]. \quad (4)$$

To isolate the effects of transmission loss due to a potentially large incident angle, we consider the power transmitted over the cross-sectional area of the incoming beam overlapping with the fiber's core by setting d to w so that Eq. (4) becomes

$$T(\theta) = \exp \left[- \frac{(\pi d\theta)^2}{4\lambda^2} \right]. \quad (5)$$

Equation (4) shows that the transmission of the unknown pulse into the fiber has a Gaussian dependence on the incident angle. If we take the acceptance angle of the fiber θ_{max} to be the full width of $T(\theta)$ at e^{-2} , then we find that it is given by $2\lambda/\pi d$. The angular window $h(k)$ is identical to $T(\theta)$ (where $\theta \approx k\lambda_0/2\pi$), and the fiber is a Gaussian angular filter. Thus, as long as we measure pulses whose NAs are less than $2\lambda/\pi d$, $E_{\text{unk}}(x, \lambda)$ will experience minimal angular filtering and be accurately sampled by the fiber because $T(\theta)$ is relatively flat in this region.

Because we know that the spatial response function is a Fourier transform of $h(k)$ we can write it as follows:

$$H(x) = \exp \left[- \frac{(2x)^2}{d^2} \right]. \quad (6)$$

If we take the spatial resolution of the fiber to be the full width of $H(x)$ at e^{-2} , then we get the expected result that it is equal to the mode diameter of the fiber (d).

Because $H(x)$ and $h(k)$ are a Fourier pair, θ_{max} is related to the mode diameter as shown above, so we can see that the acceptance angle of the fiber is determined by the mode diameter. Therefore, if we require that the focusing pulse to be measured has a NA that is less than the acceptance angle of the fiber, then we get the condition that

$$\frac{2\lambda}{\pi w} < \frac{2\lambda}{\pi d}, \quad (7)$$

where we have assumed that the focusing pulse is Gaussian with a focused spot diameter of w . From the above equation, we can see that this requirement on the NA is equivalent to requiring that the mode diameter of the fiber be smaller than the focused spot size of the pulse, which is necessary if we are to spatially resolve the incoming pulse. Therefore, if we use a fiber with sufficient spatial resolution for a given focus, then it will also have a sufficient angular acceptance. This result is equivalent to what we have intuitively argued in a previous paper [25].

In the above discussion we assumed that the incoming Gaussian beam was free of aberrations. Because aberrations will only increase the size of the focus, requiring that the fiber mode be less than the size of the focus when no aberrations are present will be sufficient. And if aberrations are present, the fiber will still accurately sample the focus.

As we have explained in Section 5, we find that it can be advantageous to measure the spectrum using the interferogram rather than directly measuring it because the spectral resolution of SEA TADPOLE can be better than

that of a spectrometer. Because we also interferometrically measure the spatial component of the focusing pulse [we reconstruct $E(x, y, z, \omega)$], we also achieve the same spatial-resolution improvement in SEA TADPOLE compared with direct measurements of $I(x, y, z)$ using the same fiber.

7. CONCLUSIONS

We have discussed a new technique (SEA TADPOLE) for measuring the spatiotemporal electric field of pulses that are complicated in space and/or time. SEA TADPOLE uses a simple experimental setup; uses a fast, direct retrieval algorithm; and has both high spectral and spatial resolution. We demonstrated that SEA TADPOLE can measure shaped pulses like those used in coherent control experiments. We also showed that SEA TADPOLE can measure the spatiotemporal field of a focusing pulse, and we illustrated this by measuring a focus with a NA of 0.085 produced by a plano-convex lens.

With simulations and measurements we illustrated that the spectrum reconstructed from a SEA TADPOLE trace is often better resolved than that measured directly with the same spectrometer. We showed that, when using SEA TADPOLE to measure a pulse, the spectrum is least distorted when there is no delay between the reference and unknown pulses.

We explained that, when using SEA TADPOLE to measure the spatiotemporal field of a focusing pulse, the NA of the focus has to be less than the NA of the fiber. We showed that this requirement is equivalent to requiring the focused spot size to be larger than the fiber's mode size.

ACKNOWLEDGMENTS

Rick Trebino, Pamela Bowlan, and Pablo Gabolde acknowledge support from National Science Foundation (NSF) Small Business Innovative Research grant 053-9595. Pamela Bowlan acknowledges support from the NSF fellowship IGERT-0221600 and thanks John Buck for helpful discussions regarding fiber coupling and Vikrant Chauhan for helpful discussion about Kostenbauder matrices. Robert J. Levis and Matthew A. Coughlan acknowledge the support of the Army Research Office through a Small Business Technology Transfer award and the National Science Foundation. We also thank Matuesz Plewicki for help calibrating the pulse shaper.

REFERENCES

1. R. Levis, G. Menkir, and H. Rabitz, "Selective bond dissociation and rearrangement with optimally tailored, strong-field laser pulse," *Science* **292**, 709–713 (2001).
2. A. Assion, T. Baumert, M. Bergt, T. Brixner, B. Kiefer, V. Seyfried, M. Strehle, and G. Gerber, "Control of chemical reactions by feedback-optimized phase-shaped femtosecond laser pulses," *Science* **282**, 919–922 (1998).
3. N. Dudovich, D. Oron, and Y. Silberberg, "Single-pulse coherently controlled nonlinear Raman spectroscopy and microscopy," *Nature* **418**, 512–514 (2002).
4. D. Meshulach and Y. Silberberg, "Coherent quantum control of two-photon transitions by a femtosecond laser pulse," *Nature* **396**, 239–242 (1998).
5. R. Trebino, *Frequency-Resolved Optical Gating: The Measurement of Ultrashort Laser Pulses* (Kluwer, 2002).
6. X. Gu, L. Xu, M. Kimmel, E. Zeek, P. O'Shea, A. P. Shreenath, R. Trebino, and R. S. Windeler, "Frequency-resolved optical gating and single-shot spectral measurements reveal fine structure in microstructure-fiber continuum," *Opt. Lett.* **27**, 1174–1176 (2002).
7. L. Xu, E. Zeek, and R. Trebino, "Simulations of frequency-resolved optical gating for measuring very complex pulses," *J. Opt. Soc. B* **25**, A70–A80 (2008).
8. D. N. Fittinghoff, J. L. Bowie, J. N. Sweetser, R. T. Jennings, M. A. Krumbügel, K. W. DeLong, R. Trebino, and I. A. Walmsley, "Measurement of the intensity and phase of ultraweak, ultrashort laser pulse," *Opt. Lett.* **21**, 884–886 (1996).
9. J. P. Geindre, P. Audebert, S. Rebibo, and J. C. Gauthier, "Single-shot spectral interferometry with chirped pulses," *Opt. Lett.* **26**, 1612–1614 (2001).
10. K. Misawa and T. Kobayashi, "Femtosecond Sangac interferometer for phase spectroscopy," *Opt. Lett.* **20**, 1550–1552 (1995).
11. A. C. Kovaecs, K. Osvay, and Zs. Bor, "Group-delay measurement on laser mirrors by spectrally resolved white-light interferometry," *Opt. Lett.* **20**, 788–791 (1995).
12. A. P. Kovaecs, K. Osvay, G. Kurdi, M. Gorbe, J. Klenbiczki, and Z. Bor, "Dispersion control of a pulse stretcher-compressor system with two-dimensional spectral interferometry," *Appl. Phys. B* **80**, 165–170 (2005).
13. D. Meshulach, D. Yelin, and Y. Silberberg, "Real-time spatial-spectral interference measurements of ultrashort optical pulses," *J. Opt. Soc. Am. B* **14**, 2095–2098 (1997).
14. E. M. Kosik, A. S. Radunsky, I. Walmsley, and C. Dorrer, "Interferometric technique for measuring broadband ultrashort pulses at the sampling limit," *Opt. Lett.* **30**, 326–328 (2005).
15. P. Bowlan, P. Gabolde, A. Schreenath, K. McGresham, and R. Trebino, "Crossed-beam spectral interferometry: a simple, high-spectral-resolution method for completely characterizing complex ultrashort pulses in real time," *Opt. Express* **14**, 11892–11900 (2006).
16. J. J. Field, T. A. Planchon, W. Amir, C. G. Durfee, and J. A. Squier, "Characterization of a high efficiency, ultrashort pulse shaper incorporating a reflective 4096-element spatial light modulator," *Opt. Commun.* **287**, 368–376 (2007).
17. M. Kempe and W. Rudolph, "Impact of chromatic and spherical aberration on the focusing of ultrashort light pulses by lenses," *Opt. Lett.* **18**, 137–139 (1993).
18. M. Kempe and W. Rudolph, "Femtosecond pulses in the focal region of lenses," *Phys. Rev. A* **48**, 4721–4729 (1993).
19. Z. Bor, "Distortion of femtosecond laser pulses in lenses," *Opt. Lett.* **14**, 119–121 (1989).
20. U. Fuchs, U. D. Zeitner, and A. Tuennermann, "Ultra-short pulse propagation in complex optical systems," *Opt. Express* **13**, 3852–3861 (2005).
21. V. V. Lozovoy, I. Pastirk, and M. Dantus, "Multiphoton intrapulse interference. IV. Ultrashort pulse spectral phase characterization and compensation," *Opt. Lett.* **29**, 775–777 (2004).
22. D. N. Fittinghoff, J. A. Squier, C. P. J. Barty, J. N. Sweetser, R. Trebino, and M. Mueller, "Collinear type II second-harmonic-generation frequency-resolved optical gating for use with high-numerical-aperture objectives," *Opt. Lett.* **23**, 1046–1048 (1998).
23. R. Chadwick, E. Spahr, J. A. Squier, and C. G. Durfee, "Fringe-free, background-free, collinear third-harmonic generation frequency-resolved optical gating measurements for multiphoton microscopy," *Opt. Lett.* **31**, 3366–3368 (2006).
24. W. Amir, T. A. Planchon, C. G. Durfee, J. A. Squier, P. Gabolde, R. Trebino, and M. Mueller, "Simultaneous visualizations of spatial and chromatic aberrations by two-dimensional Fourier transform spectral interferometry," *Opt. Lett.* **31**, 2927–2929 (2006).

25. P. Bowlan, P. Gabolde, and R. Trebino, "Directly measuring the spatio-temporal electric field of focusing ultrashort pulses," *Opt. Express* **15**, 10219–10230 (2007).
26. R. Trebino, P. O'Shea, M. Kimmel, and X. Gu, "Measuring ultrashort laser pulses just got a lot simpler," *Opt. Photonics News* **12**(6), 22–25 (2001).
27. A. E. Siegman, *Lasers* (University Science Books, 1986).
28. A. G. Kostenbauder, "Ray-pulse matrices: a rational treatment for dispersive optical systems," *IEEE J. Quantum Electron.* **26**, 1148–1157 (1990).
29. S. Akturk, X. Gu, P. Gabolde, and R. Trebino, "The general theory of first-order spatio-temporal distortions of Gaussian pulses and beams," *Opt. Express* **13**, 8642–8661 (2005).
30. K. Wicker and R. Heintzmann, "Interferometric resolution improvement for confocal microscopes," *Opt. Express* **15**, 12206–12216 (2007).
31. C. Froehly, A. Lacourt, and J. C. Vienot, "Time impulse response and time frequency response of optical pupils," *Nouvelle Revue d'Optique* **4**, 183–196 (1973).
32. L. Lepetit, G. Cheriaux, and M. Joffre, "Linear techniques of phase measurement by femtosecond spectral interferometry for applications in spectroscopy," *J. Opt. Soc. Am. B* **12**, 2467–2474 (1995).
33. P. A. Jansson, *Deconvolution with Applications in Spectroscopy* (Academic, 1984).
34. C. Dorrer, M. Joffre, L. Jean-Pierre, and N. Belabas, "Spectral resolution and sampling issues in Fourier-transform spectral interferometry," *J. Opt. Soc. Am. B* **17**, 1790–1802 (2000).
35. V. J. Coates and H. Hausdorff, "Interferometric method of measuring the spectral slit width of spectrometers," *J. Opt. Soc. Am.* **45**, 425–430 (1955).
36. V. N. Kumar and D. N. Rao, "Determination of the instrument function of a grating spectrometer by using white-light interferometry," *Appl. Opt.* **36**, 4535–4539 (1997).
37. J. A. Buck, *Fundamentals of Optical Fibers, Pure and Applied Optics* (Wiley, 2004).
38. D. Marcuse, "Loss analysis of single-mode fiber splices," *Bell Syst. Tech. J.* **56**, 703–717 (1976).